Suppression of Roughness Replication in Bilayer Films Prepared by Spin-Coating

P. Müller-Buschbaum,*,† J. S. Gutmann,†,‡ J. Kraus,† H. Walter,† and M. Stamm†,§

Max-Planck-Institut für Polymerforschung, Ackermannweg 10, 55128 Mainz, Germany, and Institut TMC, Universität Hamburg, Bundesstrasse 45, 20146 Hamburg, Germany

Received February 22, 1999; Revised Manuscript Received October 15, 1999

ABSTRACT: Utilizing the high resolution of a reflection ultrasmall-angle scattering setup, the roughness replication in polymer single-layer and bilayer samples is probed. Single films of fully brominated polystyrene (PBrS) as well as bilayer films of polystyrene on top of PBrS and of PBrS on top of polyamide-6I are investigated. Three different methods are presented to suppress the replication: the use of thick films, the use of films of laterally heterogeneous thickness, and the preparation from a solvent such that the polymer has only a weak interaction with the substrate. For single-layer samples of PBrS with increasing film thickness, the long-range correlation is decreased. Conformal roughness was detected up to a film thickness of $18R_g$ (1349 Å). At a film thickness of $26R_g$ (1989 Å), an individual scattering of the interfaces was observed. Irrespective of the roughness replication behavior of the individual sublayers, the methods presented are able to suppress the constraint of a morphology replication in bilayer films.

Introduction

Bilayer polymer films are quite frequently used in many practical applications such as coatings or adhesives. In fundamental investigations they are important as well. Some examples are the interdiffusion of two different polymer layers at their interface,[1,2] the adhesion of thin films,[3,4] and the dewetting of polymer films on top of a polymeric surface.[5,6] All these experiments consider the morphology of the polymer−polymer and the polymer−vacuum interface to be statistically independent. If a roughness replication would be present it would have implications on the further interpretation of such experiments. This results from the strong constraint that are imposed by roughness replication.[7] For example, PBrS molecules can be forced to follow the substrate morphology down to molecular in-plane lengths of R_g.[8] Additionally roughness replication was found to be present over a large range of film thicknesses and to persist until the polymer film is annealed sufficiently above its glass-transition temperature.[7] Of course the annealing of the sample is not possible in many applications of bilayer films without changing the experimental starting conditions. A way to ensure the suppression of roughness replication during the preparation is therefore interesting for many investigations.

While the roughness replication of single polymer films prepared by spin-coating was investigated recently,[7,8] we focus on the suppression of long-range correlation. We restrict ourselves to films prepared by the spin-coating technique. Quite frequently the top layer in a bilayer polymer film is floated onto the sublayer. This results in a complex roughness replication depending on the stiffness of the floated film.[9] In the presented investigation both layers, the sublayer as well as the top layer, are prepared by spin-coating. Thus comparable mechanisms for the formation of roughness replication are present. Three different methods are presented to suppress the replication without annealing: (1) The film thickness is enlarged above a typical value, which will depend on the polymer used. (2) Films with laterally heterogeneous thicknesses are prepared. (3) The interaction between the polymer and the substrate is reduced by the chosen solvent. The two examples of bilayer films presented differ in the roughness replication behavior of the sublayer before spin-coating the second layer on top of the first film. In one sample series the bottom layer is conformal with the underlying silicon substrate. In a second sample series we prepare subfilms without having conformality with the substrate. After spin-coating the second layer on top, both types of bilayer samples show no roughness replication over a wide range of investigated film thicknesses. Additionally, the measurements of the single polymer films show that the observed loss of conformality is not due to a limited resolution of the experiment. All diffuse X-ray scattering experiments presented benefit from the high resolution of a reflection ultrasmall angle-scattering (RUSAX) setup.[10] This article is structured as follows: The introduction is followed by they Experimental Section describing the sample preparation and the techniques used. The next section gives an introduction to roughness replication. Then the Results and Discussion are reported followed by Summary and Outlook.

Experimental Section

Sample Preparation. All samples were prepared on top of native oxide covered Si(100) surfaces (MEMC Electronic Materials Inc., Spartanburg). Prior to spin-coating, the silicon substrates were cleaned in a bath of 100 mL of 80% H_2SO_4, 35 mL of H_2O_2, and 15 mL of deionized water for 15 min at 80 °C, rinsed in deionized water, and dried with compressed nitrogen. The polymers used were polystyrene (PS) with a molecular weight $M_w = 30\,600$ g/mol and a narrow molecular weight distribution $M_w/M_N = 1.07$, fully brominated polystyrene (PBrS, degree of bromination $x = 1.07$) with $M_w = 144\,700$ g/mol and $M_w/M_N = 1.03$, and polyamide-6I (PA) with $M_w = 28\,900$ g/mol and $M_w/M_N = 1.10$. The amorphous polyamide is a condensate of isophathalic acid and diaminohexane (Bayer AG, Leverkusen). Three different types of sample series were

* Corresponding author. Present address: TU München, Physik-Department, LS E13, James-Franck-Strasse 1, 85747 Garching, Germany.
† Max-Planck-Institut für Polymerforschung.
‡ Universität Hamburg.
§ Present address: Institut für Polymerforschung e.V. (IPF), Hohe Str. 6, 01069 Dresden, Germany.

10.1021/ma9902551 CCC: $19.00
Published on Web 01/08/2000

Table 1. Schematic Overview of the Examined Sample Series[a]

series	sublayer	l	top layer	l
I	PBrS 145k	varied		
II	PBrS 145k	fixed	PS 31k	varied
III	PA 29k	fixed	PBrS 145k	varied

[a] The film thickness l is kept fixed or varied, respectively. The molecular weight of the samples is indicated by the numbers (in kg/mol).

investigated: (1) single films of PBrS with film thicknesses between $4R_g$ (311 Å) and $26R_g$ (1989 Å), (2) bilayer samples of PS on top of PBrS, and (3) bilayer samples of PBrS on top of PA. In both series of bilayer samples, the sublayer thickness was kept fixed and the top-layer thickness was varied. The PBrS films were prepared by spin-coating (1950 rpm for 30 s) a toluene solution of the polymer onto the silicon substrate and the PA surface. The different top films of PS were spin-coated from a cyclohexane solution ($T = 40$ °C, 1950 rpm for 30 s). Cyclohexane does not dissolve PBrS. To ensure homogeneous PA films on top of the silicon substrates, a different cleaning procedure of the substrate was necessary to achieve a hydrophilic surface: First the substrates were stored for 15 min in dichloromethane in an ultrasonic bath at about 50 °C. Afterward the wafers were washed with fresh Millipore water. The next cleaning step was an oxidation bath consisting of a mixture of 12 mL of H_2O_2, 12 mL of NH_3, and 140 mL of Millipore water at a temperature of 75 °C for 120 min. After being rinsed several times with water, the substrates were dried with clean nitrogen immediately before spin-coating PA from a 1,2-chlorophenol solution (1950 rpm for 120 s). Toluene does not dissolve PA. A schematic overview of the three different types of investigated samples is given in Table 1. Different film thicknesses were obtained by a variation in the concentration of the spin-coated solution following an empirical relation.[11]

Using X-ray reflectivity[12] the bare substrates were characterized, and the initial film thicknesses of the single and double films were determined. All diffuse X-ray scattering experiments were performed in a vacuum sample cell with a horizontally placed sample.

Optical Microscopy. The sample surfaces were observed with optical microscopy using a Zeiss Axiotech 25H optical microscope with magnifications between 4 and 50 times. A Hitachi KP-D50 CCD camera recorded the micrographs.

Specular X-ray Scattering. With X-ray reflectivity measurements at a wavelength of $\lambda = 1.54$ Å, the three different types of samples were characterized directly after preparation. The measurements were performed at a laboratory X-ray source (Seifert XRD 3003TT) with a Ge(110) channel-cut crystal monochromator operating in a two-reflection geometry and a slit collimation in front of the detector. This enables the necessary high resolution to determine the thickness of the investigated samples. From a fit to the data using a matrix formalism,[12] the laterally averaged density profile is obtained.[12−15] The model used for the fit assumes a tanh-shaped interface between individual layers of homogeneous density. If a concentration dependence of the interaction parameter χ is neglected,[16] this profile is a good approximation for the interface between polymer layers.[17] In addition, it is frequently used for silicon surfaces.[18]

Diffuse X-ray Scattering. The diffuse X-ray scattering experiments were performed at the BW4 USAX beamline of the DORIS III storage ring at HASYLAB/DESY (Hamburg). For further details concerning the beamline, see ref 19. We performed experiments at two different sample detector distances of 2870 and 11 338 mm. The first distance corresponds to a typical small-angle X-ray scattering (SAXS) experiment and the second distance to an ultrasmall angle scattering (USAX) experiment. While the instrument is normally operated in transmission geometry, we used a reflection geometry.[20] In the RSAXS setup we chose a wavelength of $\lambda = 1.38$ Å and in the RUSAX setup $\lambda = 1.13$ Å. Owing to the high-quality entrance cross-slits and a completely evacuated pathway, we were able to perform diffuse X-ray scattering under the conditions of small-angle scattering. The typical in-plane coherence length can be estimated to $\xi_{surf} \cong 500$ μm.[21] With the RUSAX setup we extended our resolution to 1.95×10^{-4} Å^{-1} (compared to 6.19×10^{-4} Å^{-1} in the RSAXS). The nonspecular as well as the specular intensity was recorded with a two-dimensional detector consisting of a 512×512 pixel array.[22] A beam-stop in front of the detector was installed at the position of the primary beam. At one fixed angle of incidence α_i, the two-dimensional intensity distribution consists of several vertical and horizontal slices. The vertical slice at $q_y = 0$ is called a "detector-scan"[23] as it is equivalent to an image obtained with a one-dimensional line detector. The (xy)-plane denotes the sample surface and $\vec{q} = (q_x, q_y, q_z)$ the scattering vector with $q = 4\pi/\lambda \sin(\alpha_i)$.

Correlated Roughness

Diffuse scattering yields information about in-plane length scales[24] and about correlation between interfaces.[25] A constructive interference between diffusely scattered beams from different interfaces leads to sheets of enhanced intensity in the reciprocal space.[26] This resonant diffuse scattering results from a full or partial correlation between different interfaces j and k. Parallel to the q_z-axis, these sheets of high intensity are in phase with the modulations of the specular reflectivity. The distance is given by $2\pi/(z_j - z_k)$ and reflects the distance $l^{corr} = z_j - z_k$ of the correlated interfaces. In a detector scan the sample is held fixed at one angle of incidence α_i and the detector position is varied around the specular peak. In a q_xq_z-map a detector scan is a parabolic path through the reciprocal space, which cuts the Yoneda as well as the specular streak. In a typical scan both peaks are visible. The intensity depends on the roughness of the sample and the chosen incident angle α_i. The Yoneda peak is a typical dynamic feature of diffuse scattering,[27] which arises from an enhancement of the scattered intensity, if the incident or exit angle equals the critical angle $\alpha_{i,f} = \alpha_c$ due to a standing wave field. In the case of correlated roughness, the intensity streaks of the resonant diffuse scattering are cut and visible as a modulation of the intensity. Additional modulations of the intensity in a detector scan may result from a dynamic effect. The standing wave field that gives rise to the Yoneda wing can cause interference fringes created by a waveguide behavior of two interfaces separated by a distance l^{dyn}. In the case of a single film on top of a semiinfinite substrate, the different angular relation of the resonant diffuse scattering and of the dynamic effect ($\Delta\alpha_f^{corr}/\Delta\alpha_i^{dyn} \cong 2$) enables a simple separation of both effects.[26] Therefore one single detector scan is sufficient to give evidence for vertical replication of roughness. Samples consisting of double-layer films have a more complex behavior owing to the additional interface. The (vacuum/polymer and polymer/polymer), the (polymer/polymer and the polymer/substrate), and the (vacuum/polymer and the polymer/substrate) interface can be correlated. Depending on the film thicknesses and scattering densities, a separation of the individual scattering contributions might be difficult. Nevertheless the absence of modulations shows that neither roughness correlation nor a waveguide behavior is present.

Results and Discussion

Specular X-ray Scattering. In Figure 1a−c reflectivity data (dots) and fits (solid lines), using the model described above, are presented. Figure 1a shows the

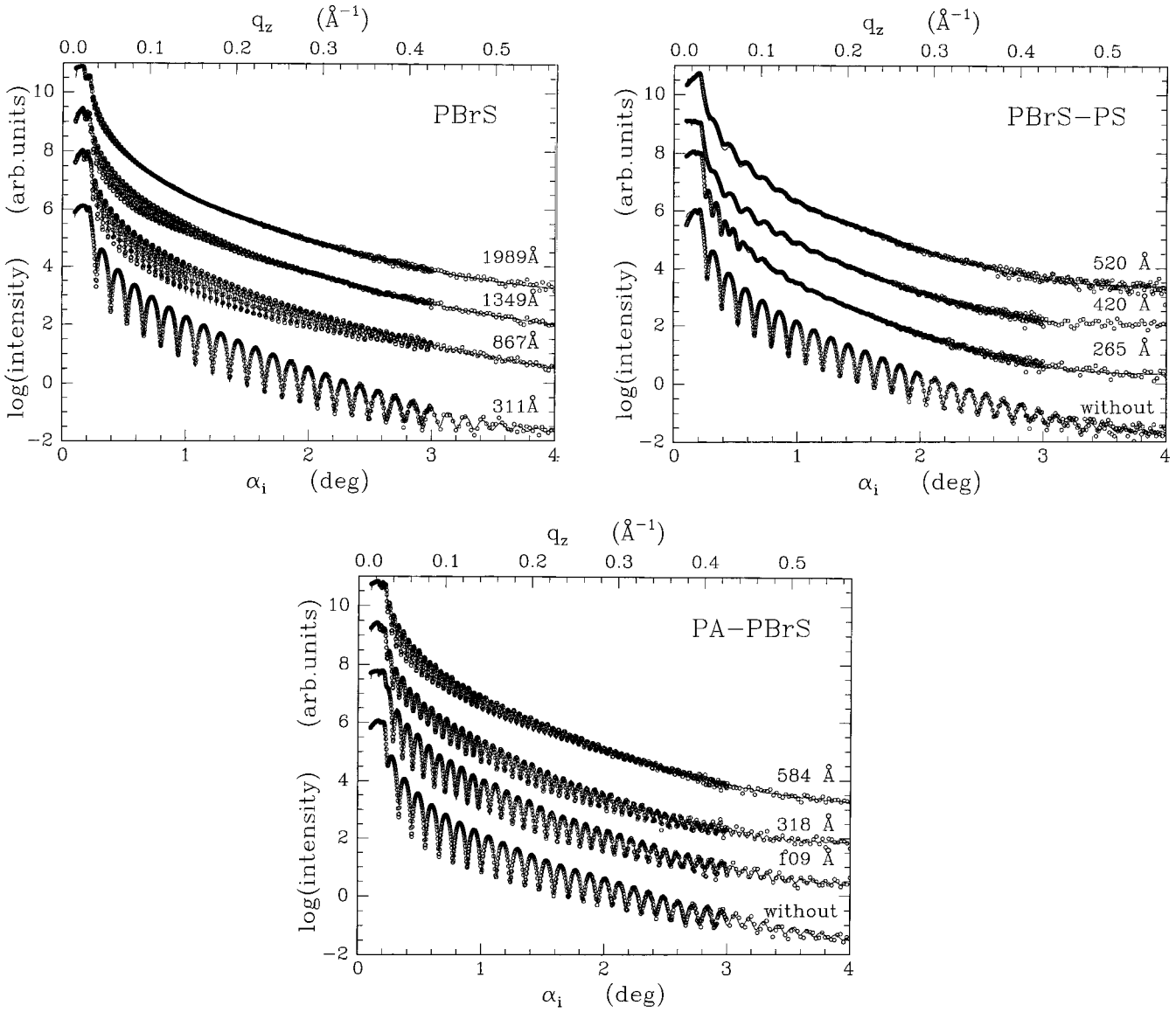

Figure 1. (a, top) X-ray reflectivity curves of single PBrS films (311, 867, 1349, and 1989 Å) on top of Si/SiO_x substrates prepared by spin-coating right after preparation. Together with the data (dots) a fit using a tanh-interface model (solid line) is shown. The curves are shifted against each other for clarity. (b, middle) X-ray reflectivity curves of bilayer samples PS on PBrS (265, 420, and 520 Å) on top of Si/SiO_x substrates prepared by spin-coating right after preparation. For comparison the single PBrS film (without) is presented, too. Together with the data (dots) a fit using a tanh-interface model (solid line) is shown. The curves are shifted against each other for clarity. (c, bottom) X-ray reflectivity curves of bilayer samples PBrS on PA (109, 318, and 584 Å) on top of Si/SiO_x substrates prepared by spin-coating right after preparation. For comparison the single PA film (without) is presented, too. Together with the data (dots) a fit using a tanh-interface model (solid line) is shown. The curves are shifted against each other for clarity.

measurements from the single PBrS films whose thickness covers a range between 311 and 1989 Å. For the molecular weight used this equals a range between $4R_g$ and $26R_g$ (R_g denotes the radius of gyration of the unperturbed molecule). The rms surface roughness of the films increases from 4 to 9 Å with increasing film thickness. In Figure 1b the single PBrS subfilm is plotted for comparison to the data of the spin-coated bilayer PBrS−PS films. Whereas the single film (thickness 314 Å) exhibits well-pronounced fringes, the fringes in the curves of the bilayer samples are strongly damped out. This results from the enhanced surface roughness of 26 up to 43 Å for the bilayer samples compared to 4 Å for the single-film surface. The prepared top-layer thickness covers a range between 265 and 520 Å. In the graph (Figure 1c) of the third type of investigated samples (PA−PBrS), similar to Figure 1b, the single PA subfilm (thickness 375 Å) and the bilayer films (thickness from 109 to 584 Å) are shown. In contrast to the measurements of the PBrS−PS samples, the ones of the PA−PBrS samples display well-pronounced fringes. The rms roughness value of the PA layer (26 Å) is larger than the one of the PBrS surface (4 Å). In addition the scattering contrast between PA and PBrS is smaller than that between PS and PBrS, which yields a reflectivity curve mainly influenced by the total film thickness.

Diffuse X-ray Scattering. We performed measurements at an angle of incident $\alpha_i > \alpha_c$ above the critical angle of total reflection of the polymer film ($\alpha_i = 0.99°$ for the RSAXS and $\alpha_i = 0.65°$ for the RUSAX setup). Therefore the typical characteristics of the scattered intensity (Yoneda peak, specular peak, modulations due to resonant diffuse scattering) can be easily separated.

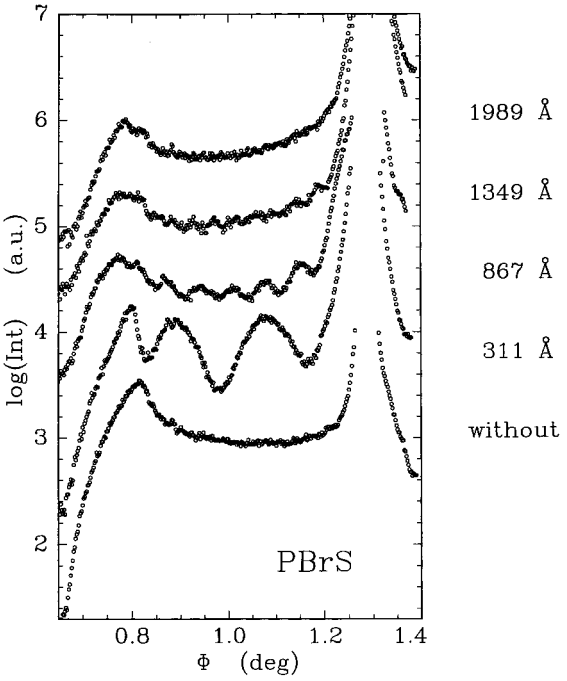

Figure 2. Detector scans measured at the angle of incidence $\alpha_i = 0.65°$ of the single PBrS films as prepared for different film thicknesses. The specular peak is cut to picture the intensity modulations due to resonant diffuse scattering more clearly. The data from the bare substrate (without) is shown for comparison. For clarity the curves are shifted by 1 order of magnitude against each other.

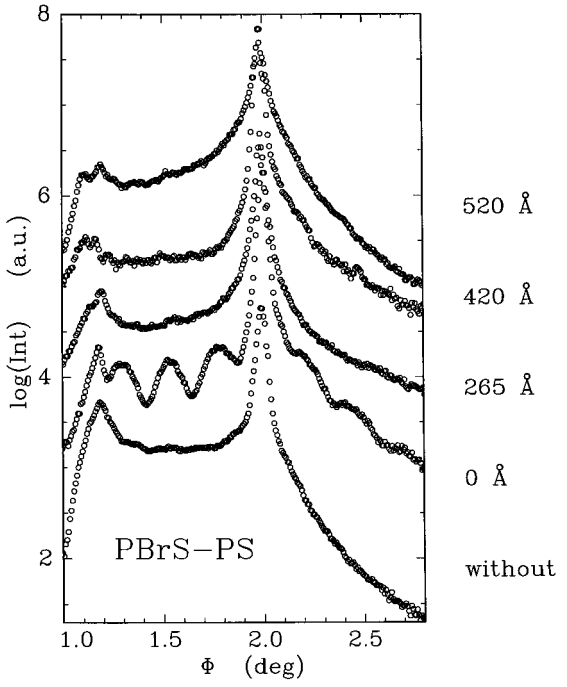

Figure 3. Detector scans measured at the angle of incidence $\alpha_i = 0.99°$ of the bilayer films PS on PBrS as prepared for different PS film thicknesses. The data from the bare substrate (without) and from the single PBrS film (0 Å) are shown for comparison. For clarity the curves are shifted by 1 order of magnitude against each other.

Figures 2−4 show detector scans as a function of the detector angle $\Phi = \alpha_i + \alpha_f$. In the RSAXS setup the intensity was integrated over $\Delta q_y = \pm 1.55 \times 10^{-3}$ Å^{-1} and in the RUSAX setup over $\Delta q_y = \pm 4.87 \times 10^{-4}$ Å^{-1}.

Unfortunately, the spin-coating process is very complicated and not fully understood. Despite its frequent use in practice, in theory it can only be modeled within a three-step model[28] including many simplifications. The first step describes the early stages, which may have no influence on the resulting structures. In the second step fluid flow reduces the amount of solvent on the rotating sample until in the third step a resulting structure is frozen in due to solvent evaporation. As reported previously[8] the correlated part of the roughness spectra of thin polymer films prepared from a toluene solution can be described as a frozen liquid with large bending rigidity. Surface structures created during the second step can be easily separated from structures installed later.[29] Owing to the fluid flow the structures formed in the second step of the spin-coating model exhibit a starlike pattern. Its center is the rotation center, and the pattern can cover the whole sample area. Surface patterns formed in the third step of the spin-coating model are homogeneous over the complete sample except a small area at the sample border, which is on the order of the capillary length. Thus these structures do not change as a function of the distance from the sample center.

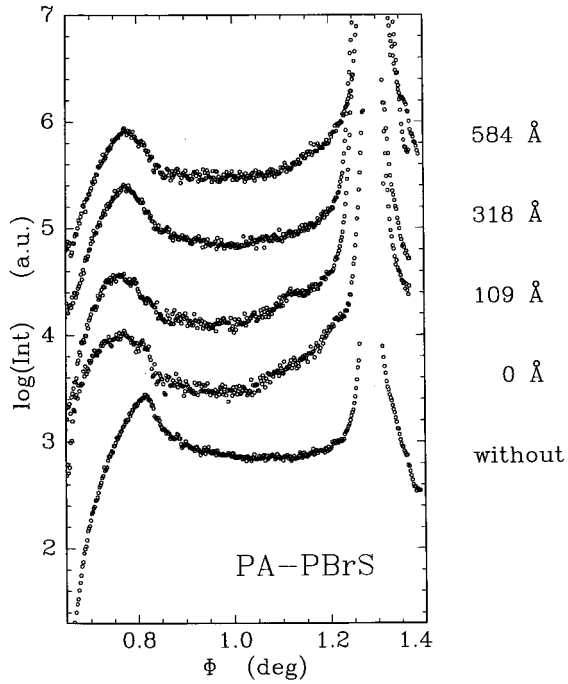

Figure 4. Detector scans measured at the angle of incidence $\alpha_i = 0.65°$ of the bilayer films PBrS on PA as prepared for different PBrS film thicknesses. The specular peak is cut to picture the intensity modulations due to resonant diffuse scattering more clearly. The data from the bare substrate (without) and from the single PA film (0 Å) are shown for comparison. For clarity the curves are shifted by 1 order of magnitude against each other.

In contrast to single-layer samples, the preparation of bilayer samples requires two individual preparation steps. Thus two times a polymer layer is spin-coated. Consequently roughness correlation can be avoided during the complete two-step preparation, or the second preparation step suppresses the long-range correlation. In this case the first prepared sublayer shows conformal roughness prior to the preparation of the second layer. Figure 5 shows both ways for bilayer samples in a schematic drawing. In the following, three different models are presented that explain the absence of roughness replication:

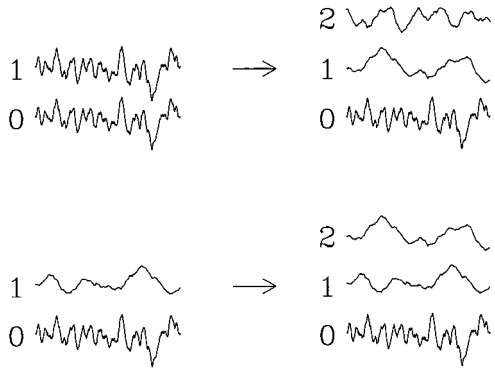

Figure 5. Schematic drawing of the interface structure of the investigated samples. Top graph (system PS on Si/SiO_x−PBrS): The single film surface (1) is correlated with the substrate interface (0). After spin-coating the second layer on top all interfaces (0, 1, 2) are independent. Bottom graph (system PBrS on Si/SiO_x−PA): Even the single-film surface (1) is independent from the substrate interface (0). In the bilayer sample no roughness replication is introduced and the interfaces (0, 1, 2) stay statistically independent.

Model 1: Large Film Thickness. Figure 2 shows the data recorded for the single PBrS films on top of Si/SiO_x to probe the large film thickness limit of roughness replication and to demonstrate the resolution of the RUSAX setup. For a comparison the data from the bare substrate (denoted without) is shown. For the molecular weight used the radius of gyration of the unperturbed molecule is R_g = 76 Å. At 311, 867, and 1349 Å well-pronounced fringes are visible while at 1989 Å no fringes between the Yoneda peak and the specular peak can be detected. The amplitude of the resonant diffuse scattering can be taken as a fingerprint of the strength of the replicated roughness. With increasing film thickness this amplitude decreases until at 1989 Å (= $26R_g$) no more fringes are visible. Thus with the RUSAX setup the limit of the long-range correlation on single films for the given molecular weight is determined. Films with larger thickness will not show correlated roughness.

Model 2: Surface Morphology Formation. Comparable single-layer films of PBrS on top of Si/SiO_x are used as substrates for the first type of bilayer samples. We chose a fixed film thickness of the PBrS layer of 314 Å. In Figure 3 the detector scan of the bare substrate (denoted without) and of the single PBrS film (denoted 0 Å) are presented. The three additional detector scans (265, 420, and 520 Å) in Figure 3 show data from the bilayer samples. On top of the PBrS film a second PS film was spin-coated out of a cyclohexane solution. Cyclohexane is expected to be a nonsolvent for PBrS and nearly a Θ-solvent for PS.[30] In contrast to the data of the single-layer sample (0 Å), which exhibits well-pronounced modulations of the intensity owing to roughness replication, none of the data from the bilayer samples shows modulations. In these detector scans only the Yoneda and the specular peak are visible. The difference of the individual Yoneda peaks stems from the different film thicknesses of the top layer. Owing to the small range of investigated film thickness, the resolution of the RSAXS setup is sufficient. Furthermore it pictures more clearly the changes of the fwhm of the specular peak owing to the large range of the detector angle Φ. With increasing PS film thickness the peak is broadened resulting from an in-plane surface morphology. On the basis of the results of the single-layer films, the formation of roughness replication for larger film thickness will become more and more unlikely. Thus by spin-coating from a cyclohexane solution we present one example to suppress roughness replication in bilayer films over a large range of film thickness. Its origin is explained with the formation of a surface morphology:

In single polymer films the installation of a marked and large surface morphology was shown to suppress roughness replication.[7] PS films spin-coated from a cyclohexane solution on top of Si/SiO_x substrates show a starlike pattern. The polymer material is concentrated in ribbonlike regions. Because the morphology is created already during the second step of the spin-coating model, the polymer surface is determined by fluid flow and the contact angle of the cyclohexane−polymer solution with the substrate. Therefore it is independent from the substrate morphology. This mechanism is the basic idea for the suppression of roughness correlation by the preparation via spin-coating even in bilayer samples (PS on PBrS). Figure 6a−d shows optical micrographs of these bilayer samples (magnification 10 times). The surface of the single PBrS subfilm is shown for comparison (Figure 6a). It looks smooth on optical length scales, while the surface of the bilayer samples (Figure 6b−d) exhibits a starlike pattern. Using a four times magnification, the center part of the sample as well as the starlike orientation of the pattern is visible (Figure 7). The sample center is placed in the center of the optical micrograph. The individual areas without polymer material are caused by hydrodynamic instabilities. Thus a roughness correlation of the top layer is suppressed owing to the formation of a fluid flow pattern, which is frozen in during the later stages of the spin-coating. Although the film thickness varies from 265 to 520 Å, the mean diameter of the surface pattern is invariant (Figure 6b−d). Only its depth increases with increasing film thickness, which is expressed in the enhanced contrast of Figure 6b−d. Consequently these structures are formed from a solvent−polymer layer of fixed thickness independent of the polymer concentration of the solution. Once created, their individual depth is determined by the polymer concentration. With increasing depth the value of the surface roughness is increased and the mean density is reduced. This explains the strong damping of the fringes in the measured reflectivity curves (Figure 1b). The absence of the roughness correlation between the subfilm and the substrate is not explainable by the formation of a surface morphology. Obviously cyclohexane is not a solvent for PBrS because we detect the sublayer with unchanged film thickness from the fit of the reflectivity curves of the bilayer samples. Additionally, the interface roughness between PBrS and PS is not enlarged compared to the value of the PBrS surface before spin-coating the second layer on top. Therefore cyclohexane may enhance the mobility of the PBrS molecules. The sample relaxes out of the constraint polymer conformation of roughness replication toward its equilibrium. This is similar to annealing above the glass-transition temperature. As a result the roughness replication is suppressed and comparable to the quenched samples after annealing.[7] It is not reinstalled after all solvent was evaporated from the sample.

Model 3: Reduced Substrate Interaction. The second type of bilayer samples examined consists of a top layer of PBrS that was spin-coated from a toluene solution on a sublayer of PA. Again the solvent used was toluene, which is expected to dissolve PBrS but not

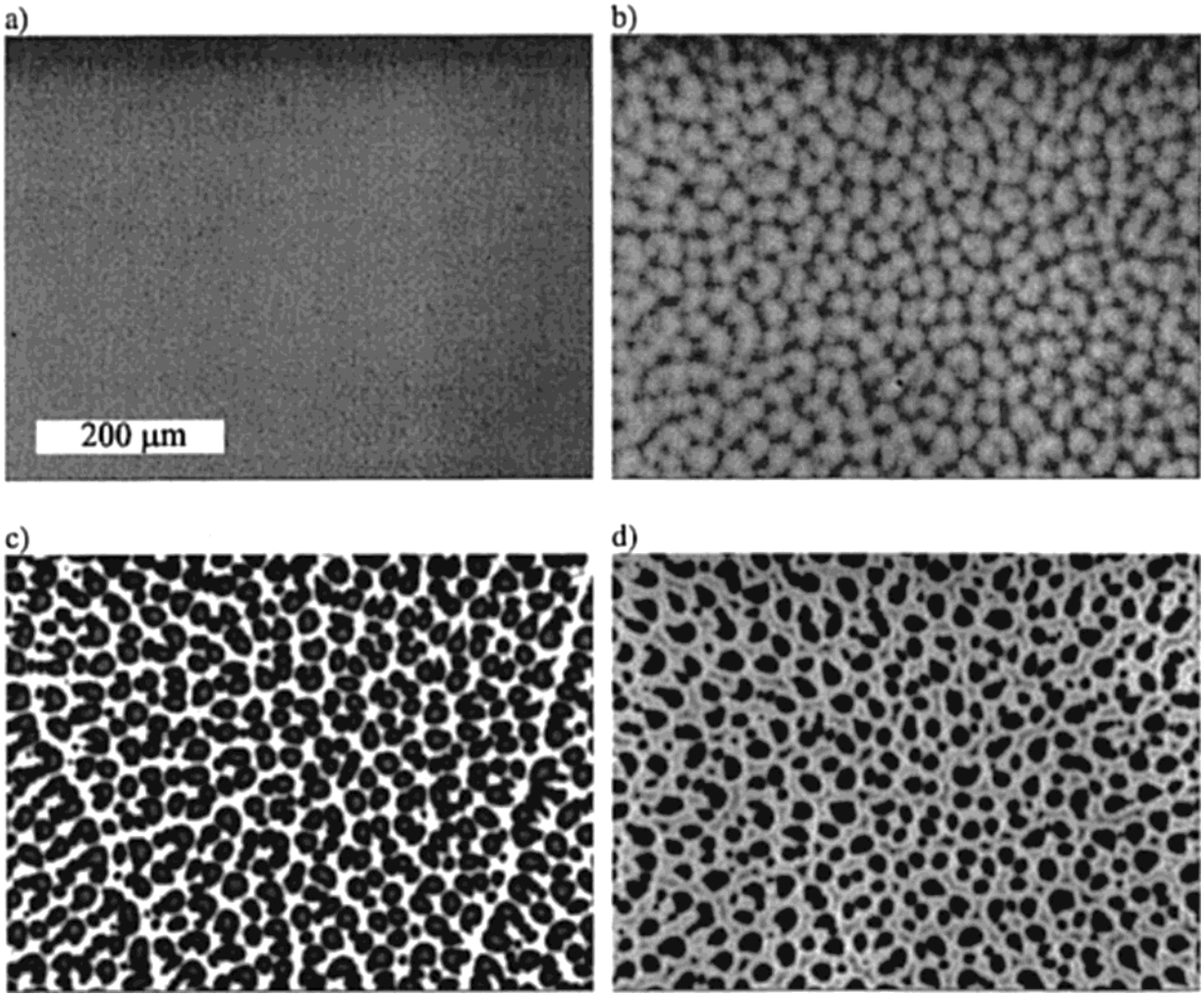

Figure 6. Optical micrographs (magnification 10 times) of the central area of the bilayer films PS on PBrS with (b) 265, (c) 420, and (d) 520 Å PS film thickness and (a) without the PS top layer. The contrast increases with increasing depth of the pattern.

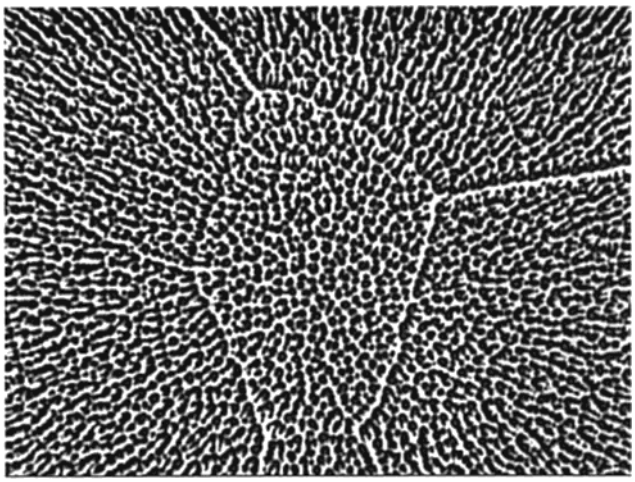

Figure 7. Optical micrograph (magnification four times) of the central area of the bilayer sample PS on PBrS with 420 Å PS film thickness.

to dissolve PA. As in Figure 3 the detector scan of the bare substrate (denoted without) of the single subfilm (denoted 0 Å) and of the three different film thicknesses of the top layer (109, 318, and 584 Å) are shown in Figure 4. Because no significant changes of the shape of the specular peak were observed with the RSAXS setup, we chose the RUSAX setup to ensure not to miss roughness replication owing to a low resolution. In contrast to the single PBrS film (Figure 3, 0 Å) the single PA film (Figure 4, 0 Å) exhibits no roughness replication and the measured detector scan shows no intensity modulations. This is a basic difference between the two samples series. The data of the bilayer samples in Figure 4 do not exhibit modulations in the diffusely scattered intensity, too. In the system PBrS on PA the scattering contrast is reduced compared to the system PS on PBrS, which makes the detection of roughness replication more difficult. In this case the internal polymer−polymer interface has only a small contribution to the complete scattering signal. This is comparable to specular scattering. Good contrast is provided from the PBrS−air interface. Nevertheless we can conclude the absence of roughness replication as resulting from the big difference in the surface roughness of the PA surface (26 Å) and the PBrS surface (4 Å). If roughness replication was present, one would obtain nearly similar values.[7,8] Thus no long-range correlation is installed by the preparation process.

Like single films of PS spin-coated out of a THF solution,[7] the PA films show no roughness replication. In both cases smooth surfaces result. No starlike pattern is detected, but the polymer surface remains independent of the substrate morphology. It results from the different interaction between the solvent−polymer solution and the substrate. The interaction between solvent and polymer molecules in this case is more favorable

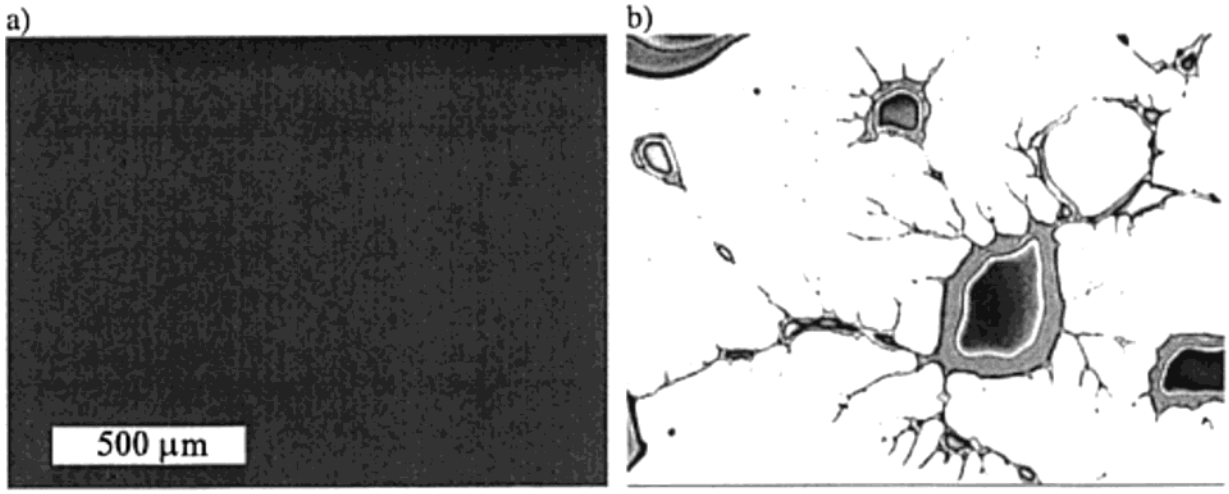

Figure 8. Optical micrographs (magnification four times) of single PA films. Depending on the surface-cleaning procedure, (a) a homogeneous film can be prepared or (b) the PA film dewets during the spin-coating.

than the interaction with the substrate. Thus the polymer molecules are not strongly attracted and constrained into an energetically unfavorable conformation, which can be assumed to be present when creating a roughness replication.[8] A further slight weakening of the interaction with the substrate results in a dewetting during the spin-coating. This is shown in Figure 8 for PA on top of Si/SiO_x. The left-hand optical micrograph (Figure 8a) shows the homogeneous PA surface prepared on Si substrates that were cleaned by the procedure described above. Without this cleaning the Si surface is not hydrophilic enough and a homogeneous PA film cannot be prepared. Figure 8b shows the resulting dewetting structure (magnification four times), which differs from the commonly observed dewetting structures.[31−33] The individual dewetting state as well as the drop diameter depends strongly on the solvent content during the third step of the spin-coating model. A reduced interaction between the polymer solution and the molecules of the underlying material may explain the absence of roughness replication of PBrS on PA, too. Comparing their surface tensions[30] and their Hamaker constants,[34] the values of PS, PBrS, and PA are very similar, whereas they differ markedly from the one of SiO_x.[35]

Summary and Outlook

In single polymer films right after preparation the roughness replication decreases with increasing film thickness. We detected a large film thickness limit of long-range correlation for the system PBrS on Si/SiO_x. Right after preparation the samples are not in equilibrium. Thus one way to overcome the constraint linked with roughness replication is the usage of films above this thickness limit. This technique works for single- as well as for double-layer samples. For samples with film thickness smaller than this limit we present two different mechanisms to suppress roughness replication. Both mechanisms work in single and bilayer polymer films directly by the preparation via spin-coating without further treatment like annealing. The first one is based on the formation of a strongly pronounced surface pattern combined with the relaxation due to enhanced mobility. It may be disadvantageous if smooth surfaces are required. The second one is based on well-balanced interactions between the molecules in a way that no interaction is strongly preferential. This limits the accessible systems to several combinations of polymers and substrates. Nevertheless compared to floated bilayer samples the preparation via spin-coating is rather quick and simple. In addition a lot of possible defects and contaminations such as water, voids, dust, or folds are minimized.

Acknowledgment. We thank C. Renger for his help during the preparation of the polyamide films and A. Zirkel for helpful discussions. Additionally we owe many thanks to S. Cunis, G. von Krosigk, and U. Lode for the technical assistance at the BW4 beamline, as well as to R. Gehrke for his general support of the experiment at HASYLAB. This work was supported by the DFG Schwerpunktprogramm "Benetzung und Strukturbildung an Grenzflächen" (Sta 324/8-1), and J.S.G. acknowledges support by the GKSS project V6.1.01.G.01-HS3.

References and Notes

(1) Stamm, M.; Hüttenbach, S.; Reiter, G.; Springer, T. *Europhys. Lett.* **1991**, *14*, 451.
(2) Karim, A.; Felcher, G. P.; Russell, T. P. *Macromolecules* **1994**, *27*, 6937.
(3) Creton, C.; Kramer, E. J.; Hui, C. Y.; Brown, H. R. *Macromolecules* **1992**, *25*, 3075.
(4) Brown, H. R.; Char, K.; Deline, V. R.; Green, P. F. *Macromolecules* **1993**, *26*, 4155.
(5) Lambooy, P.; Phelan, K. C.; Haugg, O.; Krausch, G. *Phys. Rev. Lett.* **1996**, *76*, 1110.
(6) Pan, Q.; Winey, K. I.; Hu, H. H.; Composto, R. J. *Langmuir* **1997**, *13*, 1758.
(7) Müller-Buschbaum, P.; Stamm, M. *Macromolecules* **1998**, *31*, 3686.
(8) Müller-Buschbaum, P.; Gutmann, J. S.; Lorenz, C.; Schmitt, T.; Stamm, M. *Macromolecules* **1998**, *31*, 9265.
(9) Kraus, J.; Müller-Buschbaum, P.; Stamm, M.; Bucknall, D. *J. Polym. Sci. Phys.*, in press.
(10) Müller-Buschbaum, P.; Casagrande, M.; Gutmann, J. S.; Kuhlmann, T.; Stamm, M.; Cunis, S.; von Krosigk, G.; Lode, U.; Gehrke, R. *Europhys. Lett.* **1998**, *42*, 517.
(11) Schubert, D. W. *Polym. Bull.* **1997**, *38*, 177.
(12) Lekner, J. In *Theory of Reflection*; Martinus Nijhoff Publishers: Dodrecht, 1987.
(13) Born, M.; Wolf, E. In *Principles of Optics*; Pergamon Press: Oxford, 1964.
(14) James, R. W. In *The Optical Principles of the Diffraction of X-Rays*; OxBow Press: Woodbridge, CT, 1962.
(15) Parrat, L. G. *Phys. Rev.* **1954**, *55*, 359.
(16) Binder, K.; Frisch, H. *Macromolecules* **1984**, *17*, 2928.
(17) Binder, K. *J. Chem. Phys.* **1983**, *79*, 6387.

(18) Bahr, D.; Press: W.; Jebasinski, R.; Mantl, S. *Phys. Rev. B* **1993**, *47*, 4385.
(19) Gehrke, R. *Rev. Sci. Instrum.* **1992**, *63*, 455.
(20) Müller-Buschbaum, P.; Vanhoorne, P.; Scheumann, V.; Stamm, M. *Europhys. Lett.* **1997**, *40*, 655.
(21) Salditt, T.; Rhan, H.; Metzger, T. H.; Peisl, J.; Schuster, R.; Kotthaus, J. P. *Z. Phys. B* **1995**, *96*, 227.
(22) Salditt, T.; Metzger, T. H.; Peisl, J.; Goerigk, G. *J. Phys. D: Appl. Phys.* **1995**, *28*, A236.
(23) Salditt, T.; Metzger, T. H.; Brandt, Ch.; Klemradt, U.; Peisl, J. *Phys. Rev. B* **1995**, *51*, 5617.
(24) Sinha, S. K.; Sirota, E. B.; Garoff, S.; Stanley, H. B. *Phys. Rev. B* **1988**, *38*, 2297.
(25) Daillant, J.; Bélorgey, O. *J. Chem. Phys.* **1992**, *97*, 5824.
(26) Holý, V.; Baumbach, T. *Phys. Rev. B* **1994**, *49*, 10668.
(27) Yoneda, Y. *Phys. Rev.* **1963**, *131*, 2010.
(28) Lawrence, C. J. *Phys. Fluids* **1988**, *31*, 2786.
(29) Gutmann, J. S.; Müller-Buschbaum, P.; Stamm, M. *Farady Discuss.* **1999**, *112*, 285.
(30) Brandrup, J.; Immergut, E. H. In *Polymer Handbook*; 3rd ed.; John Wiley & Sons: New York, 1989.
(31) Reiter, G. *Phys. Rev. Lett.* **1992**, *68*, 75.
(32) Reiter, G. *Langmuir* **1993**, *9*, 1344.
(33) Redon, C.; Brzoska, J. B.; Brochard-Wyart, F. *Phys. Rev. Lett.* **1994**, *27*, 468.
(34) Israelachvili, J. N. In *Intermolecular and surface forces*, 2nd ed.; Academic Press: London, 1991.
(35) Visser, J. *Adv. Colloid Interface Sci.* **1972**, *3*, 331.

MA9902551